

High-performance humidity sensor using Schottky-contacted SnS nanoflakes for noncontact healthcare monitoring

Tang, Hongyu; Li, Yutao; Ye, Huaiyu; Hu, Fafei; Gao, Chenshan; Tao, Luqi; Tu, Tao; Gou, Guangyang ;
Chen, Xianping; Fan, Xuejun

DOI

[10.1088/1361-6528/ab414e](https://doi.org/10.1088/1361-6528/ab414e)

Publication date

2020

Document Version

Final published version

Published in

Nanotechnology

Citation (APA)

Tang, H., Li, Y., Ye, H., Hu, F., Gao, C., Tao, L., Tu, T., Gou, G., Chen, X., Fan, X., Ren, T., & Zhang, G. (2020). High-performance humidity sensor using Schottky-contacted SnS nanoflakes for noncontact healthcare monitoring. *Nanotechnology*, 31(5), 1-10. Article 055501. <https://doi.org/10.1088/1361-6528/ab414e>

Important note

To cite this publication, please use the final published version (if applicable).
Please check the document version above.

Copyright

Other than for strictly personal use, it is not permitted to download, forward or distribute the text or part of it, without the consent of the author(s) and/or copyright holder(s), unless the work is under an open content license such as Creative Commons.

Takedown policy

Please contact us and provide details if you believe this document breaches copyrights.
We will remove access to the work immediately and investigate your claim.

PAPER

High-performance humidity sensor using Schottky-contacted SnS nanoflakes for noncontact healthcare monitoring

To cite this article: Hongyu Tang *et al* 2020 *Nanotechnology* **31** 055501

View the [article online](#) for updates and enhancements.





IOP | ebooks™

Bringing you innovative digital publishing with leading voices to create your essential collection of books in STEM research.

Start exploring the collection - download the first chapter of every title for free.

High-performance humidity sensor using Schottky-contacted SnS nanoflakes for noncontact healthcare monitoring

Hongyu Tang^{1,2,3,8} , Yutao Li^{2,8}, Huaiyu Ye^{4,5,6,8,9}, Fafei Hu⁶ , Chenshan Gao⁶, Luqi Tao⁶, Tao Tu², Guangyang Gou², Xianping Chen⁶, Xuejun Fan⁷, Tianling Ren^{2,9} and Guoqi Zhang^{1,9}

¹ Delft Department of Microelectronics, Faculty of Electronic, Mathematics and Information, Delft University of Technology, Delft 2628 CD, The Netherlands

² Institute of Microelectronics, Tsinghua University, Beijing 100084, People's Republic of China

³ Changzhou Institute of Technology Research for Solid State Lighting, Changzhou 213161, People's Republic of China

⁴ School of Microelectronics, Southern University of Science and Technology, Shenzhen 518055, People's Republic of China

⁵ Shenzhen Institute of Wide-Bandgap Semiconductors, Shenzhen 518055, Guangdong, People's Republic of China

⁶ Key Laboratory of Optoelectronic Technology & Systems, Education Ministry of China; College of Opto-electronic Engineering, Chongqing University, Chongqing 400044, People's Republic of China

⁷ Department of Mechanical Engineering, Lamar University, Beaumont, TX, United States of America

E-mail: h.ye@tudelft.nl, rentl@tsinghua.edu.cn and G.Q.Zhang@tudelft.nl

Received 29 May 2019, revised 7 August 2019

Accepted for publication 4 September 2019

Published 1 November 2019



CrossMark

Abstract

Humidity sensors based on flexible sensitive nanomaterials are very attractive in noncontact healthcare monitoring. However, the existing humidity sensors have some shortcomings such as limited sensitivity, narrow relative humidity (RH) range, and a complex process. Herein, we show that a tin sulphide (SnS) nanoflakes-based sensor presents high humidity sensing behaviour both in rigid and flexible substrate. The sensing mechanism based on the Schottky nature of a SnS-metal contact endows the as-fabricated sensor with a high response of 2491000% towards a wide RH range from 3% RH to 99% RH. The response and recovery time of the sensor are 6 s and 4 s, respectively. Besides, the flexible SnS nanoflakes-based humidity sensor with a polyimide substrate can be well attached to the skin and exhibits stable humidity sensing performance in the natural flat state and under bending loading. Moreover, the first-principles analysis is performed to prove the high specificity of SnS to the moisture (H₂O) in the air. Benefiting from its promising advantages, we explore some application of the SnS nanoflakes-based sensors in detection of breathing patterns and non-contact finger tips sensing behaviour. The sensor can monitor the respiration pattern of a human being accurately, and recognize the movement of the fingertip speedily. This novel humidity sensor shows great promising application in physiological and physical monitoring, portable diagnosis system, and noncontact interface localization.

Supplementary material for this article is available [online](#)

Keywords: humidity sensor, SnS nanoflakes, healthcare monitoring, noncontact sensation, Schottky-contact

(Some figures may appear in colour only in the online journal)

⁸ These authors contributed equally to this work.

⁹ Authors to whom any correspondence should be addressed.

1. Introduction

Healthcare monitoring may improve medical diagnostic efficacy and enable prediction of disease in the early stages, thereby reducing the patient numbers and finally cutting down the medical costs in the long term. Driven by the increasing demand for health monitoring and controlling, various touch-sensing devices detecting the variations of their capacitances, resistances, impedance or piezoelectricity have been reported [1–4]. In a special environment, especially in some medical circumstances, devices with the ability to sense the physiological parameters of a human being without direct contact are in great demand. Therefore, the detection of humidity becomes an efficient way to realize a noncontact interaction between a human being and electronics, which benefits disabled people [5, 6]. Thus, the search for adapt sensing materials with a high surface to volume ratio is of great importance to realize a high-quality humidity sensor with repeatable utilization and short response times.

Two-dimensional (2D) materials, graphene and transitional metal dichalcogenides (TMDCs), have been widely employed to fabricate humidity-sensing devices for health monitoring due to their high surface to volume ratios, outstanding mechanical properties, and excellent flexibility [7–13]. However, most of the pristine materials-based sensors show a long recovery time due to the chemical adsorption between water molecules and materials. Thus, surface modification and functionalization of 2D materials have been used to improve their sensing performances [14–17]. However, the fabrication process is complex and some of the functional group and doped atoms are not eco-friendly and biocompatible. According to the previous works, a humidity sensor which achieves a trade-off among high sensing performance, biocompatibility and ease of fabrication in recent research is urgently needed. Compared with them, tin sulphide (SnS) is a p-type semiconductor, which belongs to a family of layered group IV monochalcogenides and has similar puckered structures as black phosphorus [18, 19]. Its anisotropic crystal structures pose interesting anisotropic properties, such as polarized light, electric field, strain, and so on [20, 21]. Inspired by the unique electrical and physical properties, SnS has great potential application in photovoltaic converters [22], photodetectors [23], solid-state batteries [24], field-effect transistors [25], and gas detectors [26]. Especially for gas sensing between polar gas and SnS, the strong charge transfer and the adsorption-induced in-gap states can affect the carrier density and distribution in SnS and lead to outstanding sensing performances [27]. Thus, SnS nanoflakes have been used for sensing volatile compounds and noxious gas, such as acetone, alcohol [26], and NO₂ [28]. Water vapour is one kind of maximal proportion of polar gases in the air. However, the application of moisture sensing based on SnS remaining exclusive. Moreover, the SnS nanosheet exhibited good biocompatibility and has been used for cancer therapy, which makes it a good potential material for human healthcare [29].

Herein, we present a rapid response resistive humidity sensor based on mechanical exfoliated SnS nanoflakes placed on a SiO₂ and flexible substrate. The as-fabricated humidity

sensors show a room temperature water vapour sensing behaviour with short response/recovery time and broad RH range. Besides, the devices fabricated on flexible substrates are also illustrated, which show comparable sensing behaviour to the devices on rigid substrates. The humidity sensing mechanism is explained by the interactions of gas molecules (CO₂, O₂, H₂O and N₂) and SnS through first principle analysis. Finally, the fast response speed of these sensors allows us to observe a real-time dynamic monitoring of human breath and fingertip touch to demonstrate potential utilization in respiration monitoring and noncontact controlling. The achieved SnS nanoflakes-based humidity sensor with outstanding performances in the air enables its potential intelligent noncontact healthcare application.

2. Experimental details

2.1. Device fabrication

The schematic diagram of fabricating steps of a SnS nanoflakes-based sensor is shown in figure S1, available online at stacks.iop.org/NANO/31/055501/mmedia, which consists of mechanical exfoliation, transferring, and a lift-off process. The SnS bulk crystal was bought from 6Carbon Tech. Shenzhen. The SnS nanoflakes were mechanically exfoliated (ME) from the bulk crystal through thermal release tape, and then transferred onto the n++ SiO₂/Si substrate. Due to the non-uniform distributed SnS nanoflakes, we designed eight non-interconnected interdigital electrodes in one sensor for covering most of the nanoflakes. The space between the adjacent electrodes was around 5 μm. After standard photolithography, the electrodes were magnetron sputtered of Ti/Au (10/30 nm) in vacuum with a chamber pressure 6×10^{-6} Torr, and contacted with ME-SnS nanoflakes tightly. After a lift-off process, the devices were annealed at 200 °C for 2 h in argon atmosphere before testing. To fabricate the flexible sensors, we transferred the SnS nanoflakes onto a polyimide (PI) membrane by a thermal release tape (TRT)-assisted transferring technique. The PI membrane was pre-pasted on a Si wafer. After removing the residual TRT using an acetone solution, the Ti/Au electrodes were deposited onto SnS/PI substrates. Since the conductivity of Ti and Au is much larger than that of the channel material, SnS, the shape of the electrodes cannot affect the sensing performance of the resistive device.

2.2. Characterization

The optical microscopic images were acquired with an optical microscope (OLYMPUS TH4-200) imager with white light illumination using bright-field imaging modes and objectives. The thickness of the ME-SnS was determined by using an atomic force microscope (AFM, Bruker, Santa Barbara, CA, USA) and a Raman spectrometer (Raman, HORIBA, LabRAM HR Evolution) excited by a 532 nm laser. The crystalline microstructure was characterized by a transmission electron microscope (TEM, JEOL JEM-2100).

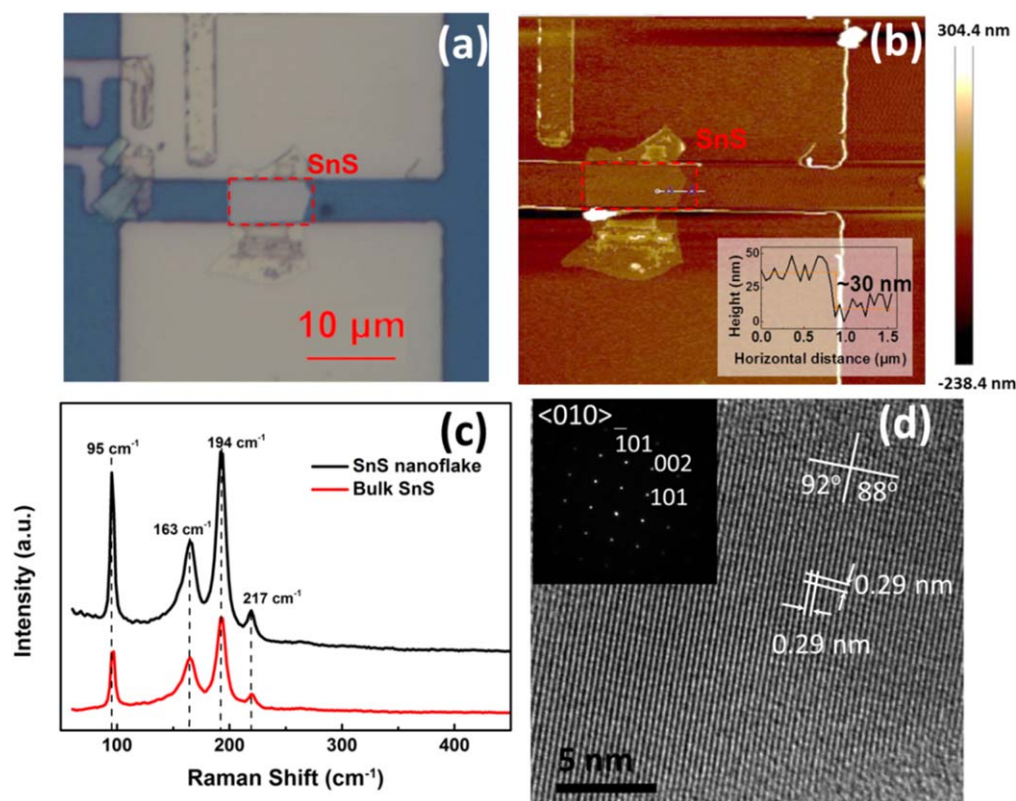


Figure 1. SnS nanoflakes deposited on a 300 nm SiO₂/Si substrate using the mechanical exfoliation method. (a) Optical image, (b) AFM image, inset image is the corresponding AFM height profile. (c) Raman image. And (d) HRTEM image with SEAD diffraction image.

2.3. Humidity test

To investigate of the effects of humidity on the electronic properties of the SnS nanoflakes-based sensor, we performed the gas sensing experiments in the AES-4TH Testing System (Beijing Elite Tech Co. Ltd). The atmospheric conditions change in the following order: ambient (25 °C, 30% RH), dry air, gradually increasing humidity (RH = 3%–99%), and ambient condition. All the gas-sensing experiments were carried out at room temperature and atmospheric pressure. Figure S2(a) shows the experimental setup used for humidity sensing performance. As shown in figure S2(b), the dry air was used as a carrier gas and injected into the chamber for 12 min to reduce the water vapour from about 80% RH down to 3% RH. Then, we varied the RH of 3%, 10%, 30%, 50%, 75% and 99% in the chamber by the mass flow controller. However, the response/recovery time is limited by the large volume of the chamber, which is about 1.5 L and needs a few minutes to be stable. Thus, we moved the sensor in/out from the bottle with dry air (3% RH) to the gas collecting bottle (99% RH) very fast for achieving accurate response/recovery time (see figure S2(c)). The RH inside gas collecting bottle was controlled by using a saturated salt solutions of potassium sulphate anhydrous (AR K₂SO₄) as described in previous literature [9].

2.4. Electrical characterization

Electrical characterization of a SnS-based device was performed using an electrical analysis system (Beijing Elite Tech

Co., Ltd, SA6101) to record the current change in real-time (data acquisition time ~30 ms). Before the gas-sensing test, the SnS-based devices were stabilized in N₂ in the system for about 30 min for fully recovering to the initial state. For the flexible SnS nanoflakes gas sensor, we applied the silver glue and fine Cu wire in the electrodes and put the flexible sensor into a 150 °C temperature chamber for 5 min. After curing and drying, the sensor was pasted to the target surface. Then, the fixed Cu wires in the positive and negative electrodes were connected with the electrical analysis system. The current–voltage (I–V) measurements were taken from –1 V to +1 V and the resistance values were calculated from the slope of the plot through the least square method. The response (S%) of SnS nanoflakes-based humidity sensor is defined as the percent change in resistance [30–34]. $S\% = (\Delta R/R_x) \times 100$, where $\Delta R = (R_{dry} - R_x)$, R_{dry} and R_x are the resistance of the sensor at dry air (3% RH) and $x\%$ RH, respectively. The sensor response and recovery time are usually defined as the time to reach 90% and 10% of the steady state signal magnitude [8, 35, 36].

3. Results and discussion

3.1. Characterization results

An optical image of the SnS nanoflakes transferred on a 300 nm SiO₂/Si substrate is shown in figure 1(a). Figure 1(b) shows the atomic force microscope (AFM) scanning image of

the SnS-nanoflakes between two electrodes. There is barely a defect and contamination on the patterned SnS surface. The inset image shows the corresponding quantitative AFM height profile. The height of the SnS nanoflake is about 30 nm [26]. The Raman spectra for the SnS nanoflake and bulk SnS were measured using a confocal Raman microprobe (see figure 1(c)). It shows the Raman peaks of SnS nanoflakes detected at 95, 163, 194, and 217 cm^{-1} , all of which match well with those from the single crystal SnS in previous literature [12, 13]. Besides, the intensity of the SnS nanoflake is much higher than that of the bulk SnS and with a small lateral shift, indicating that the nanoflake is a pure SnS crystal and with a thinner thickness than bulk SnS. As shown in figure 1(d), the high resolution transmission electron microscopy (HRTEM) image of the SnS nanoflake shows a typical d-spacing of 0.292 nm, corresponding to the distance between (101) planes of the orthorhombic phase of SnS. The inset image shows the selected area electron diffraction (SAED) pattern of SnS, which reveals a single-crystalline orthorhombic phase projected along the $\langle 010 \rangle$ direction. The interplanar angles defined by the intersection of the (101) planes of the nanoflake is 92° and 88° , which is consistent with the calculated dihedral angle between (-101) and (101) [21].

3.2. Humidity sensing performances

The sensing behaviour of a SnS nanoflakes-based humidity sensor has been measured under different RH of 3%, 10%, 30%, 50%, 75% and 99% at 25 °C. Figure 2(a) shows the rectifying output characteristics (I–V) of the device, which indicates that there exists a large Schottky barrier between SnS and the electrode. As shown in figure 2(b), we found that the resistance decreased with increasing humidity. Since H_2O is a type of charge acceptor for SnS nanoflakes, the electrons transfer from SnS to H_2O , inducing the current of SnS increases. With increasing H_2O concentration, more and more electrons discharged from SnS, thus the current increase obviously. From this plot, we noted that there is almost four orders of magnitude resistance variation exist in the as-fabricated sensor from 3% RH to 99% RH. Besides, it shows good RH-resistivity correlation under low RH, presenting potential applications in the low-humidity sensing conditions. The device is highly sensitive to environmental humidity may be attributed to the Schottky barrier modulation upon gas molecule adsorption, which is discussed in section 3.3 [37].

As a humidity sensor, the sensor has a wide RH range from 3% RH to 99% RH, and the maximum response of 2491000%, which well surpasses the humidity sensing performance of tin-based sensors. The sensor presents high response of 67600 % under 10% RH and 2491000% under 99% RH. For evaluating the response kinetics and cycling performance of the sensors, we moved the sensor in/out from the dry air (3% RH) to the gas collecting bottle ($\sim 99\%$ RH) very fast according to the saturated salt solutions method several times [9]. The cycle performance of the sensor in 3% RH and 99% RH at a bias voltage +1 V is shown in figure 2(c), indicating a repeatable and stable response of the sensor. Figure 2(d) shows the current–time (I–t) plot through

which the response and recovery time between 3% RH and 99% RH were noted as 6 s and 4 s, respectively. Compared with the reported 2D material humidity sensors (see the table S1), although the response speeds of the SnS nanoflakes-based sensor is slower than that of the graphene-based humidity sensor, it is easily fabricated and environmentally friendly. Besides, the response speed is faster than many tin-based humidity sensors [10, 38]. The sensing range is larger than those of most reported TMDC-based [9, 39, 40], nanofibers [41] and porous membrane [2] humidity sensors.

Motivated by the highly sensitive and fast response performance of the SnS nanoflakes-based sensor, we explored the possibility of whether the sensor can be fabricated on flexible substrate and enable wearable health monitoring applications. Hence, the SnS nanoflakes-based sensors on polyimide (PI) membrane substrate was demonstrated to verify the application in flexible electronics. As shown in figure S1, the fabrication process is similar with the sensor on a rigid substrate except for the step of pasting and separating PI film. The sensor can be well laminated to many curved surfaces due to the excellent flexibility of the SnS and the substrate. For instance, we pasted the flexible sensor on the surface of a finger with double-side PI tape thickness of about 200 μm and tested its current response in the flat and bend states at various RH conditions (see figure 2(e)). It was observed that the current response was slightly affected under the lower RH. When the RH exceeds 50 %RH, the current response was enhanced. In general, the distorted structure of SnS applies less adsorption site for H_2O gas molecules, while the adsorption properties of gas molecule on SnS can be significantly enhanced by applying strain [42]. Under low RH, the gas adsorption of SnS is not saturated, thus less adsorption sites induced less charge transfer between H_2O and SnS, and the current decreased slightly. Under high RH, most of adsorption sites were occupied, the high surface reactivity induced by mechanical strain can improve gas sensing behaviour, thus the current is higher than that of the flat state [39, 43]. For the dynamic RH changing test, as shown in figure 2(f), the sensor under both flat and bent conditions exhibits a repeatable response to a periodical humidity changing between 10% RH and 75% RH, showing similar sensing behaviour. Moreover, we investigated the bending performance of the SnS nanoflakes-based sensor under different bending angles and bending cycles. The results are summarized in figures S3 and S4. There is no appreciable resistance change of the flexible sensor under different bending angles. Besides, we successively carried out bending cycle test of 500 cycles of 30° , 500 cycles of 90° , 500 cycles of 120° , and 300 cycles of 180° . It found that the sensor can also be bent many times (above 500 cycles with the bending angle of 30° , 90°) without apparent degradation of response after the mechanical test (see figure S3). However, the current response of the sensor decreased after 50 bending cycles of 120° and finally failed after 300 bending cycles of 180° . It should be induced by the crack of the electrodes of sensor, which reminds us to use high flexible electrodes for enhancing the long term reliability of the device. These results clearly illustrate its ability to withstand

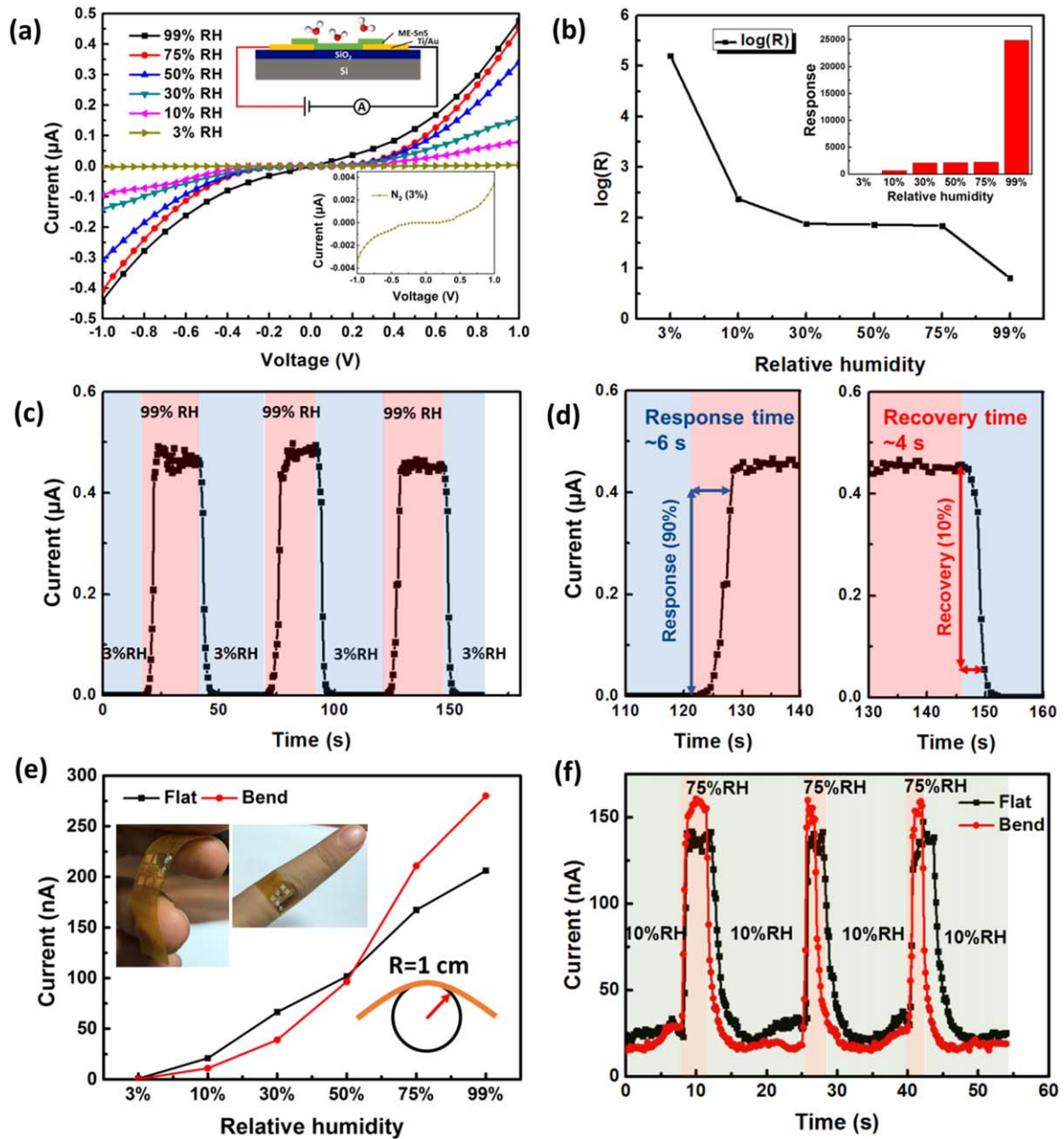


Figure 2. (a)–(d) Humidity sensing performance of the SnS nanoflakes-based sensor on rigid substrate. (a) I–V curve measured at various RH conditions, showing an obvious slope increasing with the increasing of RH. Inset top image is the schematic of SnS nanoflakes device, and the inset bottom image is the magnified curve of the 3% RH. (b) The derived RH-dependent resistance changes. Inset image is the response under different RH. (c) Time-dependent response current of three cycles of humidity switching between dry air (3% RH) and 99% RH. (d) The response and recovery time of the sensor. (e)–(f) Humidity sensing performance of the flexible SnS nanoflakes-based sensor. (e) The current response of the flexible sensor working in flat and bent states, respectively. Top left inset: image of SnS nanoflakes transferred onto the PI membrane. Top right inset: image of the flexible sensors pasted to a finger. Bottom inset: illustration of the bent state. (f) Dynamic response of the flexible humidity sensor in flat and bent states with the RH level periodically changing between 10% RH and 75% RH. All tests were conducted at room temperature of 25 °C and with a bias voltage of 1 V.

the stress of human wear in daily life, and its potential as a wearable sensing device.

3.3. Humidity-sensing mechanism

For deep learning the mechanism of the highly humidity sensitive performance of SnS-based device, we performed density functional calculations on the SnS-gas system. Of all

the gasses comprising air, CO_2 , N_2 , O_2 , H_2O , simulation of four types of gas molecules/SnS interaction can provide insight into the sensing mechanism more comprehensive. All the calculations were carried out by DMol³ code of Materials Studio [44]. Based on the density functional theory (DFT), we carried out the first-principles calculations within the generalized gradient approximated (GGA) to the Perdew-Burke-Ernzerhof (PBE) exchange-correlation functional. To

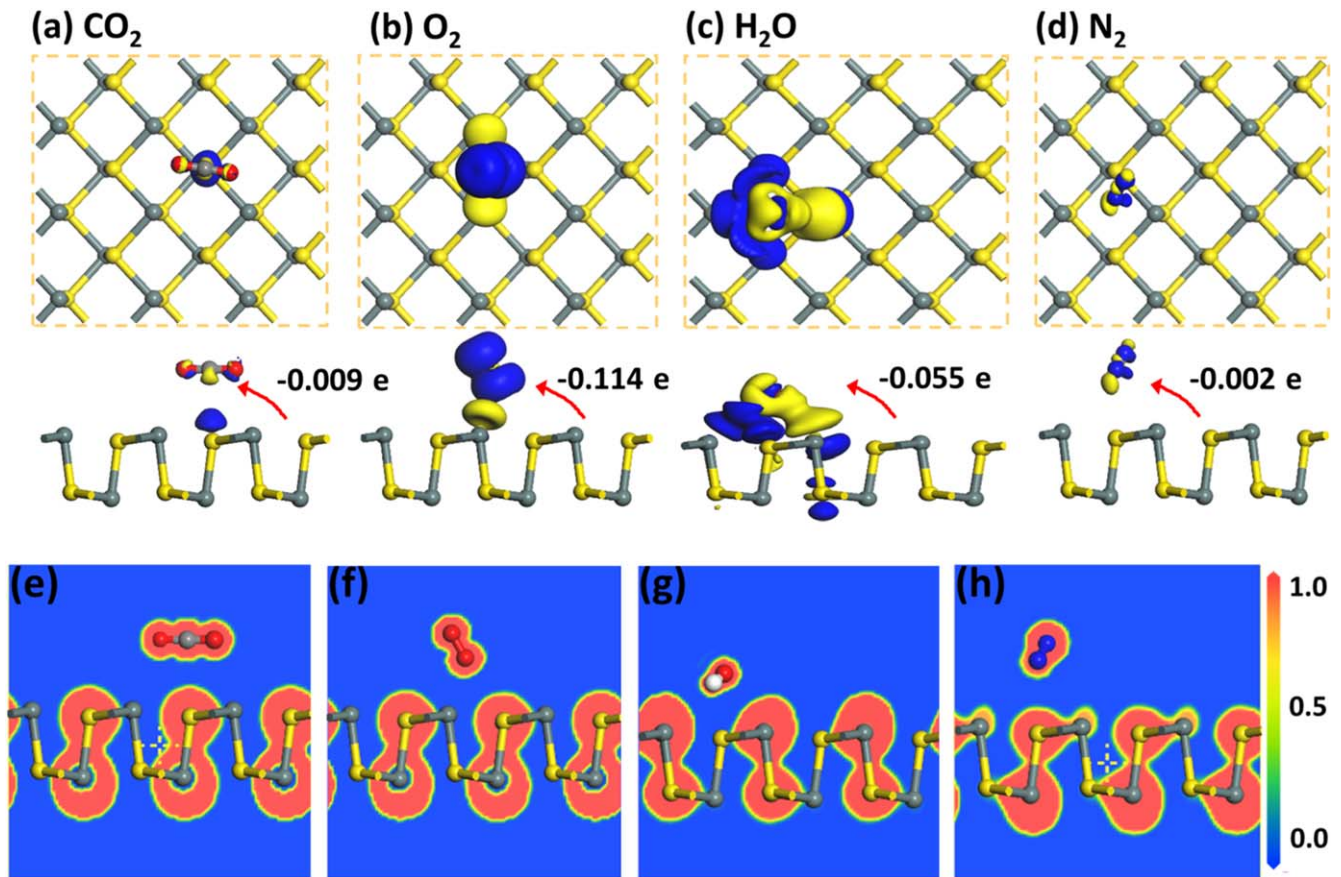


Figure 3. Top and side views of the CDD calculation for (a) CO₂, (b) O₂, (c) H₂O and (d) N₂ adsorbed on the SnS monolayer at 0 K. The isosurface is taken as $3 \times 10^{-3} e \text{ \AA}^{-3}$. The blue (yellow) region represents the charge accumulation (depletion). The negative sign of Q indicates charge transfers from SnS to the gas molecule. Electronic localization function (ELF) of (e) CO₂, (f) O₂, (g) H₂O and (h) N₂ adsorbed on the SnS monolayer. The reference bar for ELF value is provided at the right side. The balls in greyish-green and yellow balls represent the Sn and S atoms, where grey, white, red, and blue represent the Sn, S atoms, H, O, and N atoms, respectively.

better describe the van der Waals (vdW) interaction, the dispersion corrected density functional theory (DFT-D) proposed by Grimme was employed because the standard PBE functional cannot well describe the weak interactions. The all electron double numerical atomic orbital plus polarization (DNP) was used as the basis set. The kinetic energy cutoff plane wave was set to 500 eV on a Monkhorst-Pack special k-point scheme of $8 \times 8 \times 1$ for geometry optimization and $16 \times 16 \times 1$ k-points for accurate electric properties calculations. The self-consistent convergence accuracy, the maximum displacement and the convergence criterion for the force between atoms were set to be 1×10^{-6} eV per atom, 1.0×10^{-3} Å, 0.03 eV Å⁻¹, respectively. Periodic boundary conditions were applied in the x- and y- directions. A supercell with an adequate 20 Å vacuum region was introduced in the z-direction to prevent the interactions between the adjacent SnS layers, and all of the atomic positions were optimized until the maximum force is less than 0.002 Ha Å⁻¹ (see figure S5).

To better understand the interaction and quantitative determination the amount of charge transfer between gas molecule and SnS monolayer at 0 K, the charge density difference (CDD) diagram of the O atom-S site configuration is plotted in figures 3(a)–(d). The blue region represents the

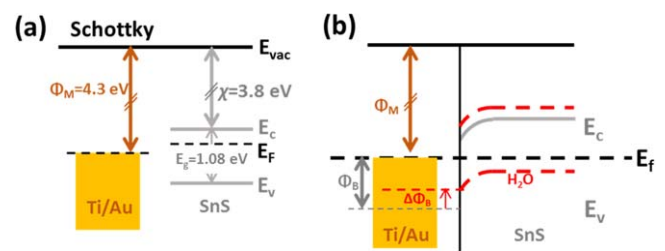


Figure 4. (a) Energy diagram of the Ti/Au and SnS before contact. (b) Band realignment and energy diagram of the Ti/Au and SnS after contact and the formation of Schottky barrier. Grey and red lines indicate the energy band of the pristine SnS (solid grey), and after exposure to H₂O (dashed red), respectively. χ is the electron affinity of SnS, E_g is the band gap, E_{vac} is the vacuum level, E_C is the conduction band minimum, and E_V is the valence band maximum. H₂O adsorption decreases the Schottky barrier (Φ_B) by $\Delta\Phi_B$, resulting in thinning of the Φ_B width and an increase of the device current.

charge accumulation, while the yellow region shows the charge depletion. It is seen that four types of gas molecule in the air (CO₂, O₂, H₂O and N₂) act as charge acceptors, and receive 0.009 e, 0.114 e, 0.055 e, and 0.002 e from single-layer SnS, respectively. In addition, as shown in figures 3(e)–(h),

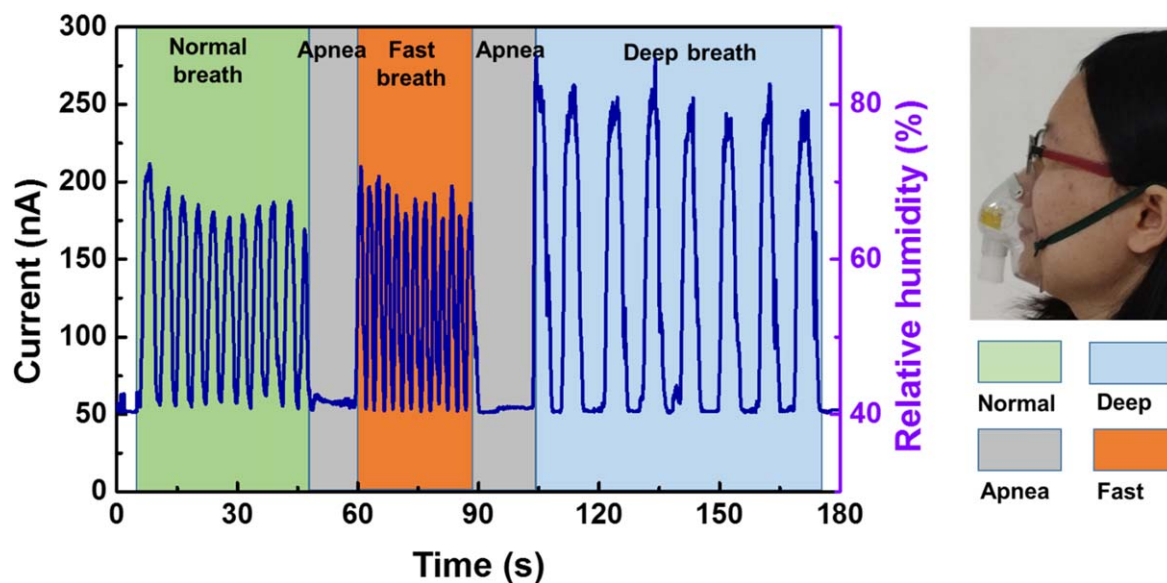


Figure 5. The current variation response to normal, deep and fast breathing at room temperature (25 °C).

it is seen that the electron localization function (ELF) has no remarkable electron sharing between gas molecules and SnS sheet, which indicates that the chemical bond is unformed. More detailed information from the simulation of different gas-SnS systems, including adsorption energy (E_A), equilibrium distances (d), and charge transfer (ΔQ) are listed in table S2 and figure S6. The d is the shortest distance between the atoms of monolayer SnS and molecule. The negative sign of Q indicates charge transfers from SnS to the gas molecule. The adsorption of H_2O on monolayer SnS produces relatively large binding energies (-0.388 eV) with charge transfer of -0.055 eV, indicating that SnS has good specificity and sensitivity for detecting water vapour in the air. Besides, a strong interaction with water molecules via physical absorption makes it possible for repeatable utilization.

From the experimental sensing results, we find that the current increased is more for high RH levels than that of lower RH levels. The sensing mechanism is relevant to the Schottky nature of SnS-metal contact (see figures 4(a), (b)). The Schottky barrier height of SnS nanoflakes-based device, Φ_B , is equal to the sum of the semiconductor band gap (E_g) and electron affinity (χ) minus the work function of the metal (Φ_M). The work function of Ti and SnS are 4.33 eV and 4.88 eV, respectively [45]. As shown in figure 4(a), it is the Schottky–Mott band alignment of Ti/Au contacts on SnS without gas adsorption. H_2O absorption moves the Fermi level of SnS toward the conduction band, decreases the Schottky barrier (Φ_B) by $\Delta\Phi_B$, resulting in thinning of the Φ_B and an increase of the device current (see figure 4(b)). For lower RH levels, because of the non-uniform distribution of water layer and non-significant charge transfer through the sensing layer, the $\Delta\Phi_B$ is small, and the response is low [16]. At higher RH levels, the SnS continuously physical adsorbs water layers, which increase the $\Delta\Phi_B$ significantly, inducing high sensitivity of the device. The recovery mechanism is also attributed to the Φ_B . When air flows out of the chamber, the

water molecule shift from the adsorption sites and the conductivity decreases due to the increased Φ_B [37, 45].

3.4. Noncontact healthcare monitoring

3.4.1. Respiration monitoring and controlling. As a benefit of its excellent performance, we intend to apply SnS nanoflakes-based humidity sensor into some medical applications, such as respiration monitoring. To investigate the respiration performance, the flexible SnS nanoflakes-based humidity sensor was used and pasted inside breath receiving mask (see figure 5). It is obvious that the sensor is sensed and recorded the breath rate and depth to the periodic exercise of normal, deep and fast breathing successfully. The apnoea process was employed during the breathing, and there is no sudden saltation for current, indicating no airflow force effects on the humidity sensor. In addition, the effect of breathing temperature difference on the response of humidity sensor can be ignored if it works at normal body temperature (figure S7). Therefore, the as-fabricated sensor is only sensitive to humidity variation at room atmospheric pressure. In all, the SnS nanoflakes-based humidity sensor shows excellent monitoring and distinction abilities for various breathing process. It is very useful for real-time monitoring the breath change during extreme sports, hazardous working environment and medical treatment. According to the signal of the breath pattern, the people can roughly predict the health condition without a region restriction, and the doctors can make a diagnosis of the breath pattern-related disease timely, such as obstructive sleep apnoea syndrome (OSAS) and asthma, etc [46, 47].

Moreover, the SnS nanoflake-based sensors have a high sensitivity in a low-humidity environment, which induce the potential application for the detection of the surface water evaporation from a fingertip. The RH and temperature near the fingertip are $\sim 40\%$ RH and ~ 30 °C, respectively. With the fingertip vertically approaching and retracting away from

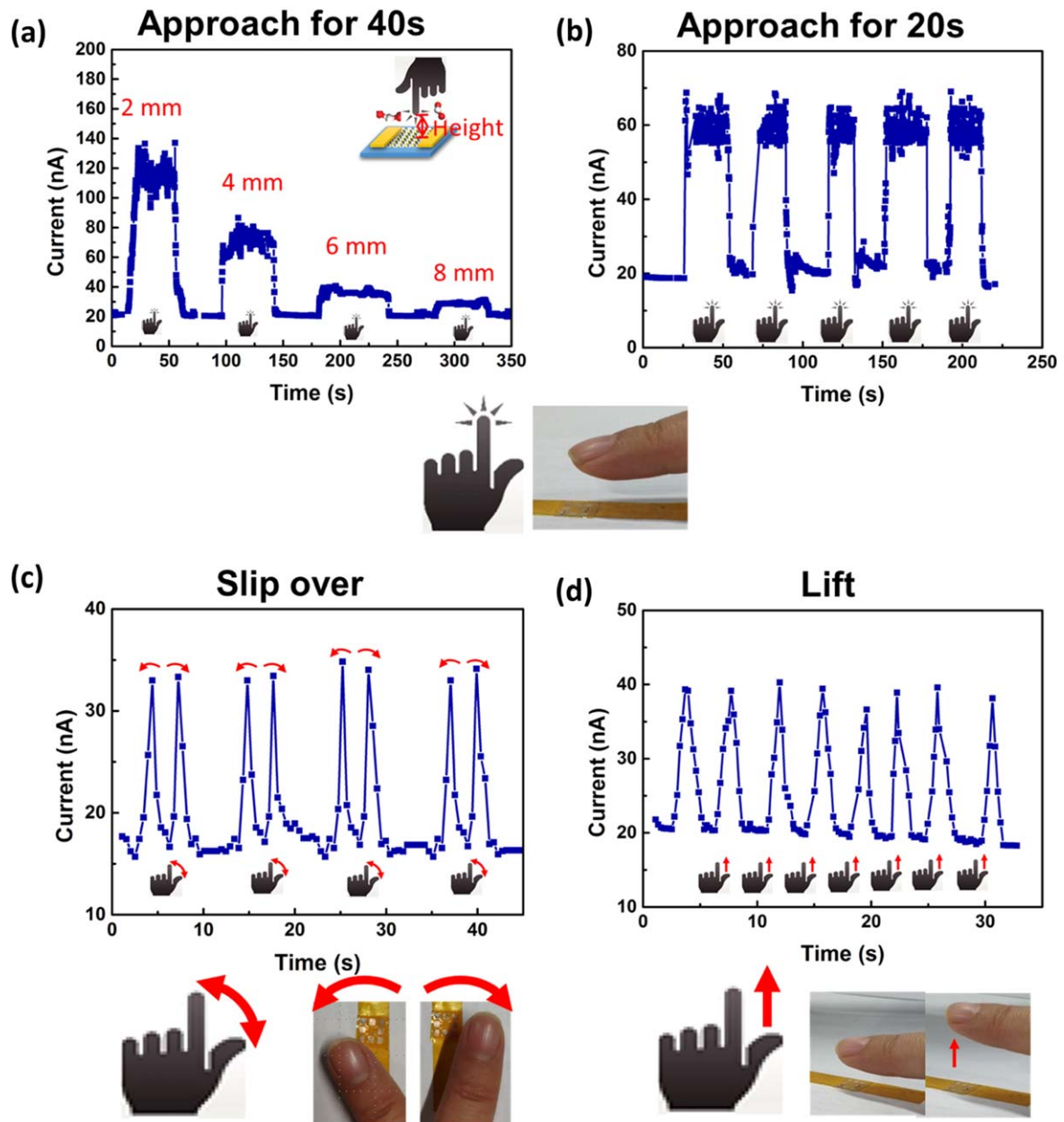


Figure 6. (a) Time-dependent response current with a fingertip vertically approaching and retracting away from the device surface at different distances. Inset: the corresponding diagram showing the configuration of the fingertip-sample distance related sensing properties. The RH of the test environment is about 30%. (b) Finger approaching for a short duration of time. (c) Quick finger slipping over the sensor. (d) Sudden finger lifting.

the device at an increasing distance, the RH of the surface of the sensor decreases, thus the response current decreases (figure 6(a)). It means that the sensor can detect a small humidity change upon a surface, implying its potential application for noncontact detection and touchscreen. As shown in figure 6(b), the sensor shows the periodical response of the finger approaching for 20 s duration time at the same height (5 mm), which is stable and repeatable. Figure 6(c) shows a quick slip of fingertip back and forth near the top of the sensor and sharp two peaks were observed, indicating a sudden shift in humidity level and a high resolution for the change of movement. Conversely, figure 6(d) shows the signals of fast lifting of a fingertip. All of the fast and stable

sensing behaviour is owed to the quick adsorption of the SnS nanoflakes to the released water vapour of the finger surface. The overall performance suggests a responsive sensitivity of the SnS nanoflakes sensor in monitoring skin evaporation for applications such as detecting gestures, physiological and physical evaluation based on perspiration, and non-invasive diagnostic of skin conditions.

4. Conclusions

In summary, we have reported an ease of fabricated Schottky-contacted SnS nanoflakes-based humidity sensors on a rigid

and flexible substrate in this work. The as-fabricated sensor exhibited good body temperature moisture sensing performance with a high response of 67600% under 10% RH and 2491000% under 99% RH, wide RH range from 3% RH to 99% RH, and fast response/recovery time of 6 s/4 s, competing with tin-based and TMDCs-based humidity sensors. The DFT analysis results suggest that the adsorption of H₂O on SnS produces relatively larger binding energies (−0.388 eV) with a charge transfer of −0.055 eV than other gas molecules in the air. The fast response and recovery performances result from the Schottky nature of SnS-Ti contact. More importantly, its wide RH range, fast response time and good biocompatibility enable real-time monitoring of finger touch without contact and different breathing patterns. Finally, this sensors shows great potential in applications in noncontact controlling and respiration monitoring from breath and finger touch experiments, which presents intelligent potential applications for noncontact healthcare monitoring.

Acknowledgments

This work was supported by the Guangdong Science and Technology Department (China) (No. 2019B010126001) and National Natural Science Foundation of China under Grant No. 51706029.

Conflicts of interest

There are no conflicts to declare.

Author contributions

H-Y Tang proposed the concept, designed and fabricated the device, performed the experiments, and contributed to the writing of the paper with equal contribution. Y-T Li proposed the designed and fabricated the device, and contributed to the writing of the paper. H-Y Ye proposed the concept and designed the device and smart home system, and discussed the manuscript. F-F Hu and C-S Gao did the first-principle analysis of SnS adsorption and prepared the manuscript. L-Q Tao and L-YW contributed to the discussions on the concept and the manuscript. T Tu and G-Y Gou performed transmission electron microscope characterizations and provided valuable discussion for the fabrication. X-P Chen and X-J Fan provided valuable discussion. Finally, T-L Ren and G-Q Zhang provided guidance to the research. All authors discussed the results and commented on the manuscript.

ORCID iDs

Hongyu Tang  <https://orcid.org/0000-0002-2720-6709>
Fafei Hu  <https://orcid.org/0000-0002-2885-541X>

References

- [1] Hu F-F, Tang H-Y, Tan C-J, Ye H-Y, Chen X-P and Zhang G-Q 2017 Nitrogen dioxide gas sensor based on monolayer SnS: a first-principle study *IEEE Electron Device Lett.* **38** 983–6
- [2] Li T, Li L, Sun H, Xu Y, Wang X, Luo H, Liu Z and Zhang T 2017 Porous ionic membrane based flexible humidity sensor and its multifunctional applications *Adv. Sci.* **4** 1600404
- [3] Parthibavarman M, Hariharan V and Sekar C 2011 High-sensitivity humidity sensor based on SnO₂ nanoparticles synthesized by microwave irradiation method *Mat. Sci. Eng. C* **31** 840–4
- [4] Tian Z, Guo C, Zhao M, Li R and Xue J 2017 Two-dimensional SnS: a phosphorene analogue with strong in-plane electronic anisotropy *ACS Nano* **11** 2219–26
- [5] Zhao J, Li N, Yu H, Wei Z, Liao M, Chen P, Wang S, Shi D, Sun Q and Zhang G 2017 Highly sensitive MoS₂ humidity sensors array for noncontact sensation *Adv. Mater.* **29** 1702076
- [6] Tai Y and Lubineau G 2017 Human-finger electronics based on opposing humidity-resistance responses in carbon nanofilms *Small* **13** -
- [7] Borini S, White R M, Wei D, Astley M, Haque S, Spigone E, Harris N, Kivioja J and Ryhanen T 2013 Ultrafast graphene oxide humidity sensors *ACS Nano* **7** 11166–73
- [8] Smith A D, Elgammal K, Niklaus F, Delin A, Fischer A, Vaziri S, Forsberg F, Rasander M, Hugosson H W and Bergqvist L 2015 Resistive graphene humidity sensors with rapid and direct electrical readout *Nanoscale* **7** 19099–109
- [9] Late D J, Huang Y K, Liu B, Acharya J, Shirodkar S N, Luo J, Yan A, Charles D, Waghmare U V and Dravid V P 2013 Sensing behavior of atomically thin-layered MoS₂ transistors *ACS Nano* **7** 4879–91
- [10] Ou J Z, Ge W, Carey B, Daeneke T, Rotbart A, Shan W, Wang Y, Fu Z, Chrimes A F and Wlodarski W 2015 Physisorption-based charge transfer in two-dimensional SnS₂ for selective and reversible NO₂ gas sensing *ACS Nano* **9** 10313
- [11] Navale S T, Mane A T, Chougule M A, Shinde N M, Kim J H and Patil V B 2014 Highly selective and sensitive CdS thin film sensors for detection of NO₂ gas *RSC Adv.* **4** 44547–54
- [12] Burungale V V, Devan R S, Pawar S A, Harale N S, Patil V L, Rao V K, Ma Y R, Eun Ae J, Kim J H and Patil P S 2016 Chemically synthesized PbS nano particulate thin films for a rapid NO₂ gas sensor *Mat. Sci.-Poland* **34** 204–11
- [13] Sagade A A and Sharma R 2008 Copper sulphide (Cu x S) as an ammonia gas sensor working at room temperature *Sensors Actuators B Chem.* **133** 135–43
- [14] Zhen Z, Li Z, Zhao X, Zhong Y, Zhang L, Chen Q, Yang T and Zhu H 2018 Formation of uniform water microdroplets on wrinkled graphene for ultrafast humidity sensing *Small* **14** 1703848
- [15] He J, Xiao P, Shi J, Liang Y, Lu W, Chen Y, Wang W, Theato P, Kuo S and Chen T 2018 High performance humidity fluctuation sensor for wearable devices via a bioinspired atomic-precise tunable graphene-polymer heterogeneous sensing junction *Chem. Mater.* **30** 4343–54
- [16] Burman D, Santra S, Pramanik P and Guha P K 2018 Pt decorated MoS₂ nanoflakes for ultrasensitive resistive humidity sensor *Nanotechnology* **29**
- [17] Zhang D, Sun Y e, Li P and Zhang Y 2016 Facile fabrication of MoS₂-modified SnO₂ hybrid nanocomposite for ultrasensitive humidity sensing *ACS Appl. Mat. Interfac.* **8** 14142–9
- [18] Tian Z, Guo C, Zhao M, Li R and Xue J 2016 Two-dimensional SnS: a phosphorene analogue with strong in-plane electronic anisotropy *ACS Nano* **11** 2219

- [19] Rodin A S, Gomes L C, Carvalho A and Castro Neto A H 2016 Valley physics in tin (II) sulfide *Phys. Rev. B* **93**
- [20] Hanakata P Z, Carvalho A, Campbell D K and Park H S 2016 Polarization and valley switching in monolayer group-IV monochalcogenides *Phys. Rev. B* **94**
- [21] Deng Z, Cao D, He J, Lin S, Lindsay S M and Liu Y 2012 Solution synthesis of ultrathin single-crystalline SnS nanoribbons for photodetectors via phase transition and surface processing *ACS Nano* **6** 6197–207
- [22] Reddy K T R, Reddy N K and Miles R W 2006 Photovoltaic properties of SnS based solar cells *Sol. Energy Mater. Sol. Cells* **90** 3041–6
- [23] Deng Z, Di C, Jin H, Su L, Lindsay S M and Yan L 2012 Solution synthesis of ultrathin single-crystalline SnS nanoribbons for photodetectors via phase transition and surface processing *ACS Nano* **6** 6197
- [24] Zhu H 2011 Elevated performances of SnS anodes with MWNTs as conductive agent for rechargeable lithium-ion batteries *Ionics* **17** 641–5
- [25] Sucharitakul S, Ulaganathan R K, Sankar R, Chou F C, Chen Y T, Wang C, He C, He R and Gao X P A 2016 Multilayer SnS field-effect transistors and the critical role of carrier screening in their performance-limit *Nanoscale* **8** 19050
- [26] Afsar M F, Rafiq M A and Tok A I Y 2017 Two-dimensional SnS nanoflakes: synthesis and application to acetone and alcohol sensors *RSC Adv.* **7** 21556–66
- [27] Hu F F, Tang H Y, Tan C J, Ye H Y, Chen X P and Zhang G Q 2017 Nitrogen dioxide gas sensor based on monolayer SnS: a first-principles study *IEEE Electron Device Lett.* **38** 983–6
- [28] Choi H, Lee J, Shin S, Lee J, Lee S, Park H, Kwon S, Lee N, Bang M and Lee S B 2018 Fabrication of high crystalline SnS and SnS₂ thin films, and their switching device characteristics *Nanotechnology* **29** 215201
- [29] Xie Z, Wang D, Fan T, Xing C, Li Z, Tao W, Liu L, Bao S, Fan D and Zhang H 2018 Black phosphorus analogue tin sulfide nanosheets: synthesis and application as near-infrared photothermal agents and drug delivery platforms for cancer therapy *J. Mater. Chem. B* **6** 4747–55
- [30] Pour G B and Aval L F 2017 Highly sensitive work function hydrogen gas sensor based on PdNPs/SiO₂/Si structure at room temperature *Results Phys.* **7** 1993–9
- [31] Behzadi Pour G 2017 Electrical properties of the MOS capacitor hydrogen sensor based on the Ni/SiO₂/Si structure *J. Nanoelectron. Optoelectron.* **12** 130–5
- [32] Behzadi Pour G and Fekri Aval L 2017 Comparison of fast response and recovery Pd nanoparticles and Ni thin film hydrogen gas sensors based on metal-oxide-semiconductor structure *Nanotechnology* **12** 1750096
- [33] Pour G B and Aval L F 2018 Monitoring of hydrogen concentration using capacitive nanosensor in a 1% H₂-N₂ mixture *Micro Nano Lett.* **13** 149–53
- [34] Pour G B, Aval L F and Eslami S 2018 Sensitive capacitive-type hydrogen sensor based on Ni thin film in different hydrogen concentrations *Current Nanosc.* **14** 136–42
- [35] Wu J, Wu Z, Xu H, Wu Q, Liu C, Yang B-R, Gui X, Xie X, Tao K and Shen Y 2019 An intrinsically stretchable humidity sensor based on anti-drying, self-healing and transparent organohydrogels *Mater. Horiz.* **6** 595–603
- [36] Buvaio A, Xing Y, Hines J and Borguet E 2011 Thin polymer film based rapid surface acoustic wave humidity sensors *Sensors Actuators B* **156** 444–9
- [37] Liu B, Chen L, Liu G, Abbas A N, Fathi M and Zhou C 2014 High-performance chemical sensing using Schottky-contacted chemical vapor deposition grown monolayer MoS₂ transistors *ACS Nano* **8** 5304–14
- [38] Parthivarman M, Hariharan V and Sekar C J M S 2011 High-sensitivity humidity sensor based on SnO₂ nanoparticles synthesized by microwave irradiation method *J. Mater. Chem. C* **31** 840–4
- [39] Guo H, Lan C, Zhou Z, Sun P, Wei D and Li C 2017 Transparent, flexible, and stretchable WS₂ based humidity sensors for electronic skin *Nanoscale* **9** 6246
- [40] Feng J, Peng L, Wu C, Sun X, Hu S, Lin C, Dai J, Yang J and Xie Y 2012 Giant moisture responsiveness of VS₂ ultrathin nanosheets for novel touchless positioning interface *Adv. Mater.* **24** 1969–74
- [41] Mogera U, Sagade A A, George S J and Kulkarni G U 2014 Ultrafast response humidity sensor using supramolecular nanofibre and its application in monitoring breath humidity and flow *Sci. Rep.* **4** 4103
- [42] Huaiyu H F Y, Tang H and Chen X 2018 Modulation of gas adsorption on snS by strain *Proc.-2018 19th Int. Conf. on Electronic Packaging Technology, ICEPT 2018* ed J W F Xiao (Shanghai: IEEE) pp 941–3
- [43] Agarwal P B, Alam B, Sharma D S, Sharma S, Mandal S and Agarwal A 2018 Flexible NO₂ gas sensor based on single-walled carbon nanotubes on polytetrafluoroethylene substrates *Flex. Print. Electron.* **3** 035001
- [44] Delley B 2000 From molecules to solids with the DMol3 approach *J. Chem. Phys.* **113** 7756–64
- [45] Hajzuz J R, Biacchi A J, Le S T, Richter C A, Hight A W and Porter L M 2017 Contacts to solution-synthesized SnS nanoribbons: dependence of barrier height on metal work function *Nanoscale* **10** 319
- [46] Pang Y, Jian J, Tu T, Yang Z, Ling J, Li Y, Wang X, Qiao Y, Tian H and Yang Y 2018 Wearable humidity sensor based on porous graphene network for respiration monitoring *Biosens. Bioelectron.* **116** 123–9
- [47] Jin H, Tao X, Dong S, Qin Y, Yu L, Luo J and Deen M J 2017 Flexible surface acoustic wave respiration sensor for monitoring obstructive sleep apnea syndrome *J. Micromech. Microeng.* **27** 115006